THERMOELASTIC INSTABILITIES IN AUTOMOTIVE DISK BRAKES — FINITE ELEMENT ANALYSIS AND EXPERIMENTAL VERIFICATION

Yun-Bo Yi
Department of Mechanical Engineering
University of Michigan
Ann Arbor, MI 48109-2125, USA

J.R.Barber
Department of Mechanical Engineering
University of Michigan
Ann Arbor, MI 48109-2125, USA

D.L.Hartsock
Ford Scientific Research Laboratories
Dearborn, MI 48121-2053, USA

Abstract

The thermomechanical feedback process due to frictional heating in sliding systems can cause thermoelastic instability (TEI), leading eventually to localization of load and high temperatures at the sliding interface. TEI in caliper/disk brake systems is an intermittent contact problem, since material points on the disk experience periods of contact with the pad alternating with periods of non-contact. The stability problem is here solved numerically by setting up a frame of reference stationary with respect to the pad and seeking a solution for the heat conduction and thermoelastic equations that varies exponentially in time. The upwind scheme is introduced in the finite element formulation to avoid possible numerical difficulties associated with the large convective terms.

A series of brake dynamometer drag tests were made to investigate experimentally the phenomenon of TEI in an automotive disk brake. The temperature field on the rotor surface was measured with infrared

(IR) detectors and a high-speed data acquisition system. The Fast Fourier Transform (FFT) method was used to determine the exponential growth rate for various hot spot numbers and critical speeds. Linear extrapolation was then used to determine the speed for zero growth rate — i.e. the critical speed. The results for critical speed and the number of hot spots show good agreement with the numerical predictions.

1. Introduction

Automotive disk brakes are susceptible to a low frequency vibration known as 'judder' or 'roughness', particularly during high speed engagement (Kubota *et al.*, 1998). Major improvements in noise reduction in other areas of automotive design have reduced customer tolerance of brake noise, resulting in a singificant volume of warranty claims associated with brake judder (Steffen and Bruns, 1998, Lee and Dinwiddie, 1998).

Various mechanisms have been proposed to account for brake judder, including rotor imbalance, non-uniform accumulation of frictional transfer films, core shift and disk thickness variation, but considerable evidence has now accumulated to show that it is associated with an unstable interaction between thermoelastic distortion and frictional heating known as *Thermoelastic Instability* or *TEI* (Jacobsson, 1999, Yi *et al.*, 2000). Temperature measurements of noisy brakes typically show a non-uniform circumferential temperature variation (Kreitlow *et al.*, 1985; Thoms, 1988, Little *et al.*, 1998) and examination of brake disks after engagement reveals evidence of focal hot spots distributed approximately evenly around the circumference (Anderson and Knapp, 1989).

The feedback mechanism responsible for TEI is illustrated by the flow diagram of Figure 1. Frictional heating during braking causes thermoelastic distortion, which in turn modifies the contact pressure distribution $p(x, y, t)$ and hence the distribution of frictional heating $q(x, y, t)$. Coupling between the mechanical and thermal problems is introduced by the energy balance relation

$$q(x, y, t) = fVp(x, y, t) \ , \tag{1}$$

where f is the coefficient of friction and V is the sliding speed. It is clear from Figure 1 that the product fV functions as the gain in the feedback process and it follows that there will generally be a critical speed $V_{\rm cr}$ above which any given sliding system will be unstable (Dow and Burton, 1972). Above the critical speed, non-uniform perturbations in the temperature field will grow, leading to a characteristic pattern of hot spots or bands on the brake disk

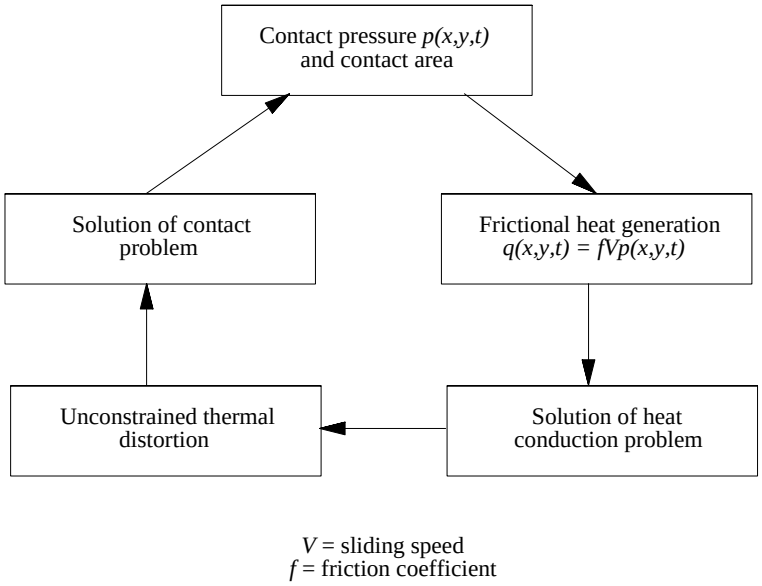

Figure 1. The feedback process for TEI.

Ideally, we would like to be able to design the brake system so that the operating conditions always lie below V_{cr}. However, V_{cr} is significantly affected by the geometry of the system (Lee and Barber, 1993) and hence it is generally necessary to use numerical methods (typically the finite element method) to obtain appropriate design estimates. Two broad categories of numerical solution have been attempted. In *numerical simulations*, the system is discretized by the finite element method and the nodal temperatures are evaluated after each of a succession of small time increments using an updating algorithm (Zagrodzki, 1990). In the alternative *eigenvalue formulation*, Burton's method is generalized to determine the conditions under which a small perturbation in the discretized temperature field can grow exponentially in time (Du *et al.*, 1997). In both methods, difficulties are encountered due to the relative motion of the brake components which introduces convective terms into the governing equations for at least one body. Peclet numbers are generally high, leading to the confinement of the thermal disturbance in a thin layer of the pad material and necessitating a very fine local mesh. Yi *et al.* (2000) showed that non-axisymmetric perturbations on an otherwise axisymmetric brake or clutch system can be analyzed by considering perturbations of Fourier form. In this case, analysis for each Fourier number is restricted to the two-dimensional cross-sectional plane, in which there is no convection. However, this method cannot be

used for typical caliper disk brakes, since the perturbations will generally not then have Fourier form.

In the present paper, we shall extend Yi's method to fully non-axisymmetric systems, which will necessitate appropriate discretization of equations with convective terms at high Peclet number. We shall compare the predictions with a set of experiments on commercial disk brakes using infrared (IR) temperature measurement to determine in each case critical speed and dominant mode shapes.

2. The automotive disk brake

Figure 2 shows the main features of a typical automotive disk brake. Two brake pads make contact with the two plane surfaces of the rotating disk, the surface facing out from the vehicle being known as the *outboard* surface and the other as the *inboard* surface. Most disks contain air vents at the mid-plane for cooling purposes, but it should be remarked that the practical heat transfer coefficients are not sufficient to enable significant cooling to occur during the brake engagement. The principal function of the cooling vents is to accelerate cooling of the disk in the usually longer periods of time *between* engagements. The disk is connected to the axle by a *hat section* and the precise way in which this is connected to the disk can have a significant effect on thermoelastic distortion. The brake pads are pressed against the disk surfaces by hydraulic pressure through a caliper mechanism, designed to equalize the forces on the inboard and outboard sides. However, this equalization is usually achieved by a sliding mechanism and this may lock due to frictional effects during loading, preventing the system from responding to changes in pad loads during a single engagement. This can have a significant effect on the stability of modes involving small numbers of hot spots.

3. Finite element determination of critical speed

For the disc brake system, we use a cylindrical polar coordinate system r, ϕ, z, fixed with respect to the caliper and brake pads. The eigenvalue solution is then obtained by postulating the existence of a perturbation in the temperature field of the form

$$T(r, \phi, z, t) = \Re\{e^{bt}\Theta(r, \phi, z)e^{bt}\} \tag{2}$$

involving exponential growth with time t. If this form is substituted into the various governing equations and boundary conditions of the processes described in Figure 1, the exponential factor will cancel, leaving a homogeneous problem defined in the spatial domain r, ϕ, z, with the possibly complex growth rate b as a parameter. The finite element

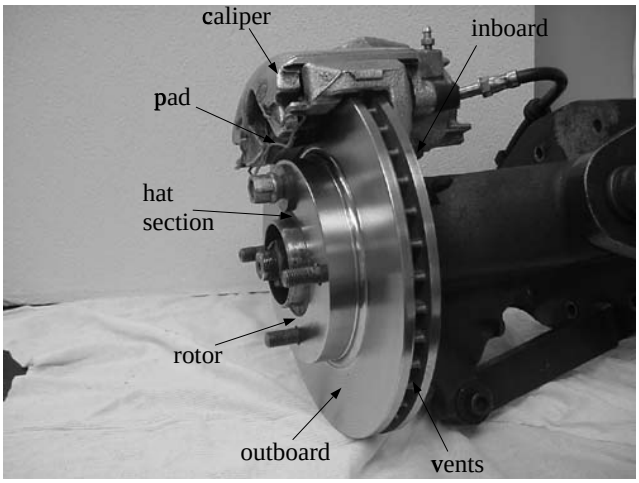

Figure 2. A typical automotive disk brake.

method is then used to discretize these equations, leading to a linear eigenvalue problem for b. The system is unstable if there exists any eigenvalue b with positive real part, since any slightly perturbed initial condition could be expressed as an eigenfunction expansion.

3.1. The heat conduction problem

The temperature perturbation in must satisfy the heat conduction equation

$$K_\beta \nabla^2 T - \rho_\beta c_\beta \left(\frac{\partial T}{\partial t} + \omega_\beta \frac{\partial T}{\partial \phi} \right) = 0 \,, \tag{3}$$

where $K_\beta, \rho_\beta, c_\beta$ are the thermal conductivity, density and specific heat respectively of material β and ω_β is the angular velocity of body β in the given frame of reference. If we denote the rotor as $\beta = 1$ and the pad/caliper assembly as $\beta = 2$, then ω_1 will be the rotational speed of the rotor and ω_2 will be zero.

Substituting (2) into (3), cancelling the common exponential factor and discretizing the resulting equation be the finite element method leads to the matrix equation

$$(\boldsymbol{K} + \boldsymbol{C} + b\boldsymbol{H})\boldsymbol{\Theta} + \boldsymbol{Q} = 0 \,, \tag{4}$$

where $\boldsymbol{\Theta}$, $\boldsymbol{Q}$ are the vectors of nodal temperatures and nodal heat sources respectively,

$$\boldsymbol{K} \;=\; \int_\Omega K_\beta \left(\frac{\partial \boldsymbol{W}}{\partial r}\frac{\partial \boldsymbol{N}^T}{\partial r} + \frac{1}{r^2}\frac{\partial \boldsymbol{W}}{\partial \phi}\frac{\partial \boldsymbol{N}^T}{\partial \phi} + \frac{\partial \boldsymbol{W}}{\partial z}\frac{\partial \boldsymbol{N}^T}{\partial z} - \frac{\boldsymbol{W}}{r}\frac{\partial \boldsymbol{N}^T}{\partial r} \right) d\Omega$$

$$\boldsymbol{H} = \int_\Omega \rho_\beta c_\beta \boldsymbol{W}\boldsymbol{N}^T d\Omega \tag{5}$$

$$\boldsymbol{C} = \int_\Omega \rho_\beta c_\beta \omega_\beta \boldsymbol{W}\frac{\partial \boldsymbol{N}^T}{\partial \phi} d\Omega$$

and $\boldsymbol{N}(r,\phi,z), \boldsymbol{W}(r,\phi,z)$ are vectors of shape and weight functions respectively.

The nodal heat sources $\boldsymbol{Q}$ are non-zero only at the contact interface, where they result from frictional heating. For the disc brake geometry, the sliding speed V varies with radius r, being given by $V = \omega r$. The discrete form of equation (1) is therefore

$$\boldsymbol{Q} = f\boldsymbol{V}\boldsymbol{\Phi}\tilde{\boldsymbol{P}} \,, \tag{6}$$

where $\tilde{\boldsymbol{P}}$ is the nodal contact force normal to contact interface which is defined only at the N_c contact nodes, $\boldsymbol{V}$ is the diagonal $N_c \times N_c$ matrix defined by

$$V_{ji} = \omega r_i \delta_{ji} \,, \tag{7}$$

$\boldsymbol{\Phi}$ is an $N_c \times N$ matrix defined by

$$\boldsymbol{\Phi} = \begin{bmatrix} \boldsymbol{I} \\ 0 \end{bmatrix} \,, \tag{8}$$

and $\boldsymbol{I}$ is the identity matrix of order $N_c \times N_c$.

3.2. Upwind finite element scheme

Numerical solutions of the convective-diffusion equation tend to exhibit unacceptable oscillations when the Peclet number characterizing the convective term is sufficiently large (Christie *et al.* 1976). This is almost always the case for brake problems, where typical Peclet numbers are of the order of 10^5. Galerkin-type finite element formulations result in expressions similar to those of central difference, which become unstable when the *element* Peclet number

$$\mathrm{Pe}_{\mathrm{el}} = \frac{Vh}{k} > 2 \,, \tag{9}$$

where h is the element dimension and k is the thermal diffusivity.

Christie *et al.* (1976) and Heinrich *et al.* (1977) showed that this difficulty could be avoided by using linear shape functions N_i, but special weighting functions of the form

$$W_i = W_i(x,\alpha) = N_i \pm \frac{3\alpha x(x-h)}{h^2} \,, \tag{10}$$

where x $(0 < x < h)$ is a local coordinate, This reduces to the Galerkin form when the upwind factor α is zero, whereas $\alpha = 1$ gives a fully upwind scheme. Corresponding weighting functions for two and three-dimensional problems can be obtained in the same way. For example, for a bilinear quadrilateral element we obtain

$$W(\xi,\eta) = \begin{bmatrix} \left(\frac{(1-\xi)}{2} - \frac{3\alpha(1-\xi)(1+\xi)}{4}\right)\frac{(1-\eta)}{2} \\ \left(\frac{(1+\xi)}{2} + \frac{3\alpha(1-\xi)(1+\xi)}{4}\right)\frac{(1-\eta)}{2} \\ \left(\frac{(1+\xi)}{2} + \frac{3\alpha(1-\xi)(1+\xi)}{4}\right)\frac{(1+\eta)}{2} \\ \left(\frac{(1-\xi)}{2} - \frac{3\alpha(1-\xi)(1+\xi)}{4}\right)\frac{(1+\eta)}{2} \end{bmatrix}, \tag{11}$$

where $\xi \in (-1,1)$ and $\eta \in (-1,1)$ are dimensionless local coordinates in and perpendicular to the convective direction respectively. The resulting shape and weighting functions are compared in Figure 3 for $\alpha = 1$.

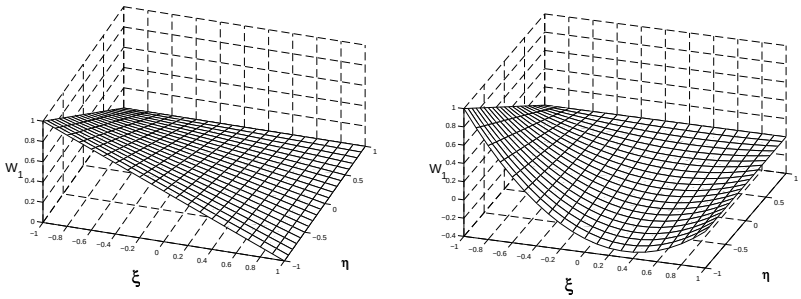

(a) Linear weighting function (b) Upwind weighting function

Figure 3. Comparison of the shape function and the upwind weighting function for a bilinear quadrilateral element.

3.3. The thermoelastic contact problem

To complete the feedback loop in Figure 1, we need to solve a thermoelastic contact problem to determine the contact pressure distribution $p(x,y,t)$ due to a given instantaneous temperature field $T(x,y,z,t)$. As long as full contact is maintained, this is a problem in linear thermoelasticity which in discrete form corresponds to a matrix equation of the form

$$\tilde{\boldsymbol{P}} = \boldsymbol{A}\boldsymbol{\Theta}\ , \tag{12}$$

where $\boldsymbol{A}$ is an $N \times N_c$ matrix relating the vector of N nodal temperatures $\boldsymbol{\Theta}$ to the vector of N_c nodal normal forces at the contact nodal pairs. Yi

et al. (2000) describe various methods of determining the matrix $\boldsymbol{A}$, but the most efficient is to develop a custom finite element description of the thermoelastic contact problem. Details of this process are omitted here in the interests of brevity.

3.4. The eigenvalue equation

Eliminating $\boldsymbol{Q}$ and $\tilde{\boldsymbol{P}}$ between equations (4,5,10), we obtain

$$[(\boldsymbol{K} + \boldsymbol{C} + fV\boldsymbol{\Phi}\boldsymbol{A}) + b\boldsymbol{H}]\boldsymbol{\Theta} = 0\,, \tag{13}$$

which is a generalized linear eigenvalue equation for the exponential growth rate b. The matrices are not symmetric and the eigenvalues are generally found to be complex. Instability is indicated if at least one eigenvalue has positive real part. The corresponding eigenfunction $\boldsymbol{\Theta}$ then defines the form of termperature perturbation that will develop.

The factor ω in equation (11) shows that the eigenvalues and eigenfunctions will depend on rotational speed. The critical speed $\omega_{\rm cr}$ can be determined by iteration until the the dominant eigenvalue has zero real part. In practice it is found that the growth rate varies approximately linearly with speed above the critical speed, so a good estimate is obtained by making a single linear extrapolation through growth rates for two super-critical speeds.

4. Experimental investigation

The evolution of hot spots in a caliper disc brake during drag braking was monitored using an array of fiber optic cables connected to single point, two colour, infrared (IR) detectors. The detectors were housed in liquid nitrogen cooled dewars to maintain a constant temperature. Five sensors were arranged along a radial line on each of the inboard and outboard sides of the rotor. During braking, each sensor sweeps the entire circumferential distribution of temperature at a given radius with every revolution, permitting a time history of the complete surface temperature distribution to be reconstituted from the recorded data.

The use of two colour detectors reduces the sensitivity of the system to emissivity, but does not completely eliminate it. The system was therefore calibrated against a set of thermocouples embedded 0.5 mm below each surface of the disk. The rotor was subjected to 200 burnish stops and several long drags to condition the surface. It was then heated to 600^oC by dragging at low speed and calibration readings were taken during subsequent cooldown at 30 rmp with the brakes released and no external cooling air. During this period, the surface of the rotor was assumed to be the same temperature as the thermocouples due to the

high conductivity of the cast iron and the slow rate of cooling. A ninth order poynomial was used to fit the data for each IR detector, a typical calibration curve being shown in Figure 4.

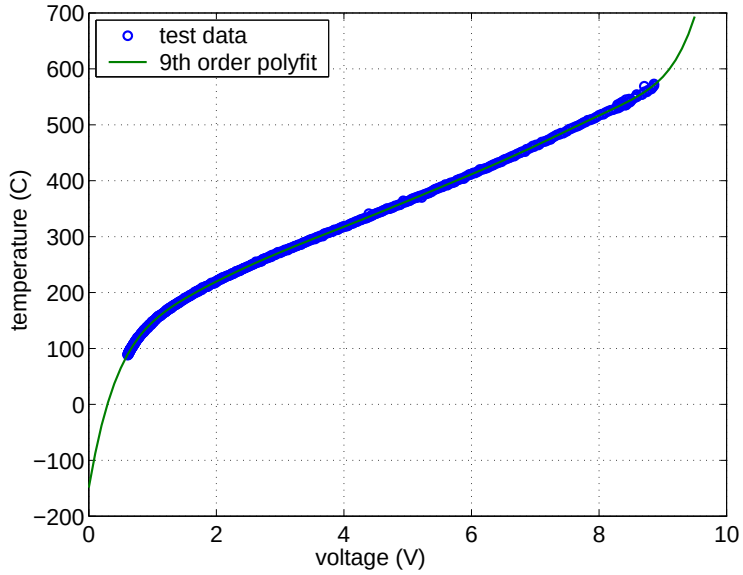

Figure 4. Calibration curve for one of the IR sensors.

The IR system was set to take temperature readings at a frequency of 2000 Hz, which corresponds to one reading every 4.2 degrees of rotation at the highest rotational speed used (1400 rpm). This was considered to give adequate resolution of the spatial distribution of temperature for typical hot spot patterns.

Figure 5 shows a typical instantaneous temperature distribution. The temperature field is clearly periodic, so it is convenient to separate components of different wavenumber in the digital data using Fast Fourier Transformation (FFT). The amplitude of a typical Fourier mode is plotted logarithmically against time in Figure 6. This particular component only begins to rise out of the noise level after about 60 s of sliding. There is then an approximately linear portion of the curve, corresponding to exponential growth, after which the growth levels off, probably because contact between the pad and the rotor becomes localized in hot spots, resulting in a strong non-linearity (Zagrodzki *et al.*, 2001). An exponential growth rate was estimated for each Fourier mode by fitting a straight line to the logarithmic plot in the growth phase, as shown in Figure 6.

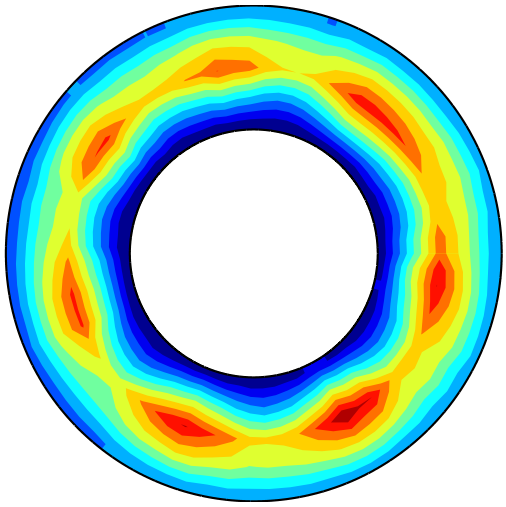

Figure 5. Typical instantaneous temperature field due to TEI.

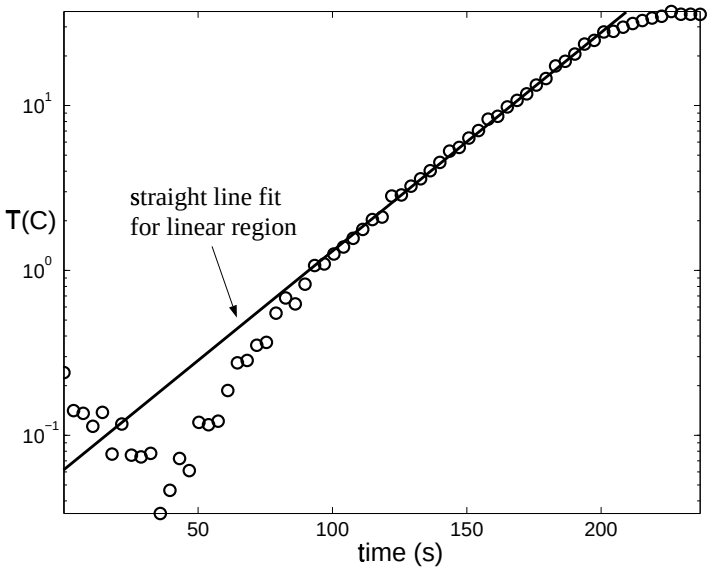

Figure 6. Logarithmic plot of average amplitude against time for the mode $n = 7$. The slope of the straight line fit corresponds to a growth rate $\Re(b) = 0.0368\ \mathrm{s}^{-1}$.

4.1. Test procedure

Whenever a new set of hardware was installed, it was subjected to a program of 200 burnish stops to condition the pad/rotor interface.

Temperature measurements were then made during a sequence of drag braking (constant speed) tests in order of increasing sliding speed. Since the probability of TEI increases with speed, this procedure eliminates the possibility that TEI at a higher speed would precondition the rotor at a particular wavenumber resulting in false indications of TEI at lower speeds. A typical test sequence is shown in Table 1.

Table 1. Typical test sequence.

Sections	Type	Speed (rpm)	Torque (ft-lb.)
1	200 Burnish stops		
2∼4	3 Drag tests	416	187.5
5	20 Burnish stops		
6∼8	3 Drag tests	555	140.6
9	20 Burnish stops		
10∼12	3 Drag tests	694	112.5
13	20 Burnish stops		
14∼16	3 Drag tests	833	93.75

Notice that the friction torque was controlled so as to maintain the same rate of power dissipation (and hence heat generation) in each test. This ensures that the evolution of the mean temperature of the brake system is approximately the same for each test and reduces the impact of temperature dependent material properties on the stability behaviour. The tests were repeated on different sets of hardware to ensure repeatability.

5. Results and discussion

For all the brake systems tested, hot spots were clearly identifiable when the sliding speed was sufficiently high. The number of hot spots developed was quite reproducible for a given brake design and the final pattern usually involved a number of equal spaced focal hot spots located approximately midway between the inner and outer radii of the rotor. However, the scenario of hot spot development showed some variability. In some cases, hot spots started near the outer edge and progressed inwards, whilst in others they started near the inner edge and progressed outwards. This movement was believed to be the result of pad wear and warpage during the long drag. Although there was no fixed location

where the hot spots would start, there was a tendency to develop a hot band near the outer radius of the rotor, probably as a result of the higher local sliding speed. This band then frequently started to exhibit variations which would develop into hot spots.

Results from each drag test were used to obtain exponential growth rates of all Fourier modes following the procedure illustrated in Figure 6. The critical speed for each mode was then estimated by linear extrapolation through the results for the speeds with identifiable exponential growth.

5.1. Comparison of experimental results and theoretical predictions

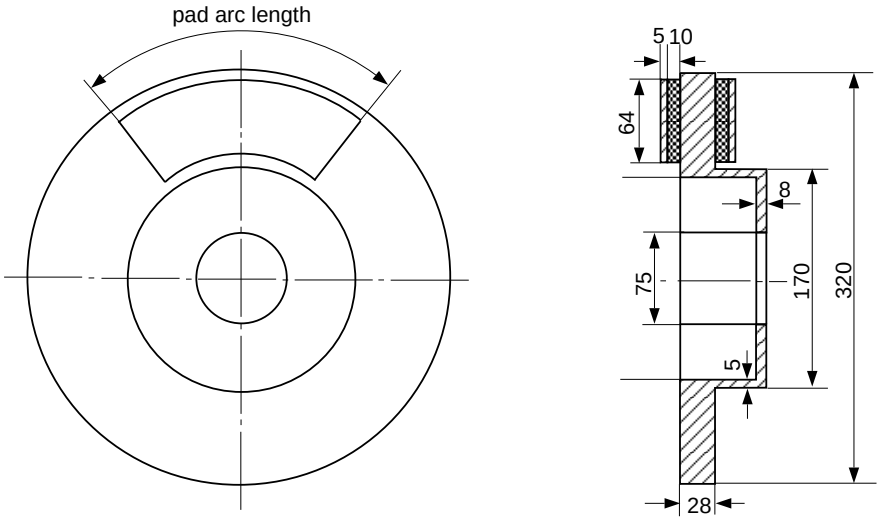

Figure 7. Dimensions of the brake system (in mm).

The dimensions of the basic brake design tested are shown in Figure 7. The rotor contains 37 vents (not shown in Figure 7) of thickness 12 mm. The vent:vane ratio is 4:1 and hence the vents occupy 80% of the total circumference of the rotor at the mid-plane. For the standard brake, the pad arc length $\phi_p = 66^o$, but tests were also conducted on brakes with reduced arc lengths of 53^o and 40^o. Other design modifications tested included the reduction of the total rotor thickness d_r (by machining a standard rotor) from 28 mm to 21 mm and of the pad friction material thickness d_p from 10 mm to 5 mm.

Theoretical predictions of the critical speed were obtained using the finite element method of section 3. In order to model the vents, 74

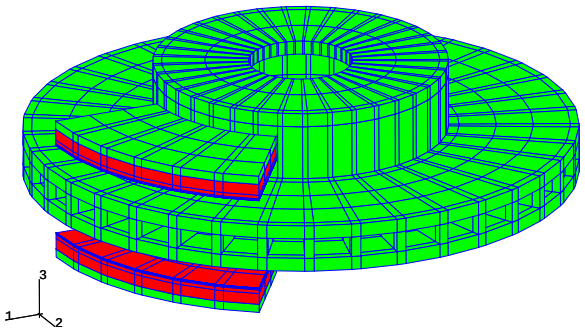

Figure 8. Finite element discretization of the brake system.

elements were used around the circumference of the disk, resulting in the model of Figure 8, which contains about 3000 eight node solid elements. Some approximation is involved in this representation of the vents, since in reality the vent boundaries move in the given frame of reference. However, numerical studies show that the temperature perturbation is largely concentrated near the rotor surface, so the resulting error is not expected to be large. An alternative strategy would be to estimate the properties of an 'equivalent homogeneous material' to replace the vent/vane region. The material properties used in the numerical solution are given in Table 2 and the coefficient of friction was taken as $f = 0.4$, based on experimental measurements. The pad modulus was obtained by ultrasonic measurements through the thickness direction, since this mode of deformation dominates the pad deformation.

Table 2. Material properties.

	E GPa	ν	α $\times 10^{-6}$deg K^{-1}	K W/m deg K	k mm^2/s
Rotor	112.4	0.25	13.25	57.0	17.2
Pad	2.03	0.35	30.0	0.93	0.52
Backing plate	200	0.3	12.0	42.0	11.9

Figure 9 compares experimental estimates of the critical speed for each wavenumber with theoretical predictions for a brake with pad arc angle $\phi_p = 66^o$, pad thickness $d_p = 10$ mm and rotor thickness $d_r = 21$ mm. The dominant mode for this brake involves 7 hot spots, for which the estimated experimental critical speed is $V_{\rm cr} = 348$ rpm. The finite

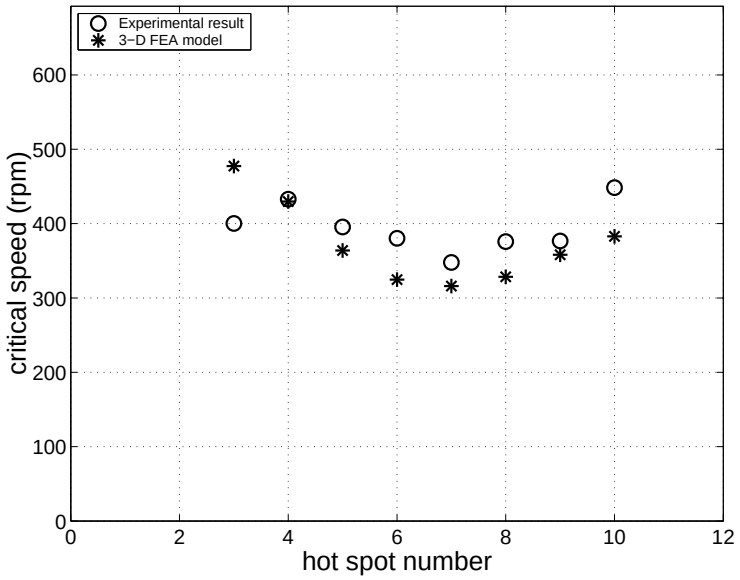

Figure 9. Comparison of experimental estimates and finite element predictions of critical speeds for various wavenumbers.

element method also predicts 7 hot spots, with a critical speed of $V_{\rm cr}^* = 316$ rpm.

Similar comparisons were performed for brakes with other values of the parameters ϕ_p, d_p, d_r and the results are summarised in Table 3. In all cases the predicted number of hot spots n^* is within ± 1 of the experimentally observed value and the maximum error in the predicted critical speed is 27%, which represents an exceptional level of agreement for such a complex problem.

The experimental results show that reducing the pad arc angle ϕ_p from 66^o to 53^o has comparitively little effect on the critical speed, but that a further reduction to 40^o increases it by a factor of 2.4. This increase is associated with an increase in the number of hot spots from 7 to 10, which is close to the minimum number that ensures that at least one hot spot is located in the contact zone at all times (Lee and Barber, 1993).

Reducing the pad thickness d_p reduces the critical speed significantly. This is attributable to the increased stiffness associated with the thinner layer of compliant friction material. It suggests that brakes are more likely to exhibit judder when the brake pads are significantly worn.

These effects are clearly identified by the finite element analysis. Other investigations, not reported here, have shown that the FEA correctly

Table 3. Comparison of experimental results ($V_{\rm cr}$) and theoretical predictions ($V^*_{\rm cr}$) of critical speed.

ϕ_p mm	d_p mm	d_r mm	V rpm	n	b $\rm s^{-1}$	$V_{\rm cr}$ rpm	$V^*_{\rm cr}$ rpm	n^*	Error
66	10	21	555	7	0.022	348	316	7	9.2%
66	10	21	694	7	0.037				
53	5	28	555	7	0.057	233	274	8	17.9%
53	5	28	694	7	0.067				
53	10	28	555	6	0.007	342	435	7	27.1%
53	10	28	694	6	0.012				
66	10	28	555	6	0.016	324	281	7	13.3%
66	10	28	694	6	0.026				
40	10	28	833	10	−0.001	833	726	10	12.7%
40	10	28	971	10	0.043				

also identifies the effect of changes in the geometry of the hat section on susceptibility to judder.

6. Conclusions

We have shown that a finite element implementation of the eigenvalue method gives generally excellent predictions of the critical speed for TEI for a caliper disc brake and also successfully identifies the effect of minor design changes on the critical speed. The analysis of one brake design by this method takes about 5 hours CPU time on a workstation. By contrast, no results have been reported for direct numerical simulation of a brake system with anything like the present level of geometric detail. We conclude that the eigenvalue method is the best numerical tool for TEI brake design presently available.

Acknowledgments

The authors are pleased to acknowledge support from the Ford Motor Company and from the National Science Foundation under contract number CMS-9619527.

References

Anderson, A.E. and Knapp, R.A. (1990) Hot spotting in automotive friction systems, *Wear* **135**, 319–337.

Christie, I., Griffiths, D.F., Mitchell, A.R. and Zienkiewicz, O.C. (1976) Finite element methods for second order differential equations with significant first derivatives, *International Journal for Numerical Methods in Engineering,* **10**, 1389–1396.

Dow, T.A. and Burton, R.A. (1972) Thermoelastic instability of sliding contact in the absence of wear, *Wear* **19**, 315–328.

Du, S., Zagrodzki, P., Barber, J.R. and Hulbert, G.M. (1997) Finite element analysis of frictionally-excited thermoelastic instability, *J. Thermal Stresses* **20**, 185–201.

J.C.Heinrich, J.C., P.S.Huyakorn, P.S. and O.C.Zienkiewicz, O.C. (1977) An 'upwind' finite element scheme for two dimensional convective transport equation, *International Journal for Numerical Methods in Engineering*, **11**, 131–143.

Jacobssen, H. (1999) Analysis of brake judder by use of amplitude functions, *SAE* 99-01-1779.

Kreitlow, W. Schrödter, F. and Matthäi, H. (1985) Vibration and hum of disc brakes under load, *SAE* 850079.

Kubota, M., Suenaga, T. and Doi, K. (1998) A study of the mechanism causing high speed brake judder, *SAE* 980594.

Lee, K. and Dinwiddie, R.B. (1998) Conditions of frictional contact in disk brakes and their effects on brake judder, *SAE* 980598.

Lee, K. and Barber, J.R. (1993) Frictionally-excited thermoelastic instability in automotive disk brakes, *ASME J. Tribology* **115**, 607–614.

Little, E., Kao, T-K., Ferdani, P. and Hodges, T. (1998) A dynamometer investigation of thermal judder, *SAE* 982252.

Steffen, T., and Bruns, R. (1998) Hot spot formation on passenger car disks, *ATZ Automobiltechnische Zeitschrift* **100**, 408–413.

Thoms, E. (1988) Disc brakes for heavy vehicles, *Proc.Int.Conf. Disc Brakes for Commercial Vehicles*, Inst.Mech.Eng. (London), C464/88, 133–137.

Yi, Y-B., Barber, J.R. and Zagrodzki, P. (2000) Eigenvalue solution of thermoelastic instability problems using Fourier reduction, *Proc.Roy.Soc. (London)* **A 456**, 2799–2821.

Zagrodzki, P. (1990) Analysis of thermomechanical phenomena in multidisc clutches and brakes, *Wear* **140**, 291–308.

Zagrodzki, P., Lam, K.B., Al-Bahkali, E.and Barber, J.R. (2001) Nonlinear transient behaviour of a sliding system with frictionally excited thermoelastic instability, *ASME J. Tribology*, in press.